Robust Controllers Enhanced With Design and Implementation Processes

Vilma A. Oliveira, *Member, IEEE*, Eduardo S. Tognetti, and Daniel Siqueira

Abstract—In this paper, instructional material on the design of robust controllers that applies to introductory graduate or advanced undergraduate courses on control is provided. The main objective is the presentation of key concepts and interpretations that help students learn robust control design. The use of recently developed techniques in robust control such as H_∞, μ analysis, and synthesis is explored. Emphasis is given to the modeling of the robust control problem with the system requirements described in a unified approach using weighting functions and linear fractional transformations (LFTs). Also, the results of a conventional lead–lag are included to reinforce the concept of robustness. The students should understand the basics of robust control using the MATLAB/Simulink platform and a hardware-in-the-loop experiment with a magnetic levitation system, which is considered a good plant for analysis and control design since it is a nonlinear unstable plant with practical use in high-speed transportation and magnetic bearings. The hardware-in-the-loop experiments are suitable for assessment during the final two semesters of engineering courses and are useful to further develop the students' skills in control engineering. The control algorithms are evaluated in the LabVIEW environment, which introduces the students to industrial platforms.

Index Terms—Control design, control education, robust control, stability and performance robustness, μ synthesis.

I. INTRODUCTION

MANY successful applications of robust control have been reported in the literature, and several control textbooks now include robust control techniques [1]–[3]. Because robust control is highly mathematical, one finds quite a challenge to balance theory and practice in undergraduate courses. In this paper, instructional material enhancing class and laboratory work with MATLAB and LabVIEW, showing the applicability of advanced control techniques, is provided. A magnetic levitation (maglev) device that is commonly encountered in undergraduate laboratories is used. Recently, several papers on education using a maglev device for enhancing control courses have appeared [4]–[6]. In these papers, the effective usage of a real-time digital control environment with a hardware-in-the-loop maglev device for reinforcement of modeling and control education is demonstrated.

In this paper, the focus is on robust control analysis and design. Design and implementation issues of robust controllers

and the use of μ analysis to check the stability and performance robustness of the solutions are addressed. To alleviate the mathematics involved, the concepts of robust control are introduced with the help of block diagrams and transfer functions. The general control structure and analysis of solutions with different controllers lead to several class activities, and the student is expected to develop MATLAB programs and Simulink diagrams following the guidelines included. To facilitate the prompt reproduction of the class activities developed, the main MATLAB commands and Simulink diagrams are provided.

The paper is organized as follows. In Section II, stability and performance concepts for a typical control system structure are presented. In Section III, some of the mathematics involved in the design of robust controllers are presented in the framework of linear fractional transformations (LFTs), with the general block structure for robust control introduced step by step using the usual system descriptions. Section IV presents the system equations and linearized model about an operation point. The design steps, which include the main MATLAB functions and Simulink diagrams developed, are provided in Section V. In Section VI, class assignments are provided, and in Section VII, the digital implementation setup and typical experimental results are given. Finally, some concluding remarks are included in Section VIII.

II. STABILITY AND PERFORMANCE

In this section, the key concepts in robust control to be learned by the students are summarized. The students are expected to review the subjects of singular value decomposition and matrix norms. From the feedback system shown in Fig. 1(a), one obtains the relations $r - y = Sr$, $y = Tr$, $u = KSr$, which yield the feedback transfer matrices from r to each of the outputs $e := r - y$, y and u, respectively, with

$$S(s) := (I + G(s)K(s))^{-1}$$
$$T(s) := G(s)K(s)(I + G(s)K(s))^{-1} = I - S(s) \quad (1)$$

where $G(s)$ is the nominal plant and $K(s)$ the controller. The matrices S and T are referred to as sensitivity and complementary sensitivity matrices, respectively. Since $e = Sr$, the sensitivity matrix S determines the steady-state behavior of the feedback system. The relations $y = Sd$ and $y = SGd_i$ obtained from Fig. 1(a) imply that the sensitivity matrix S also determines the disturbance attenuation. Therefore, to reflect disturbance attenuation and steady-state specifications, one usually specifies an upper bound on the norm of $S(j\omega)$, that is

$$\bar{\sigma}\left(S(j\omega)\right) \leq \left|W_1^{-1}(j\omega)\right|, \quad \forall \omega \qquad (2)$$
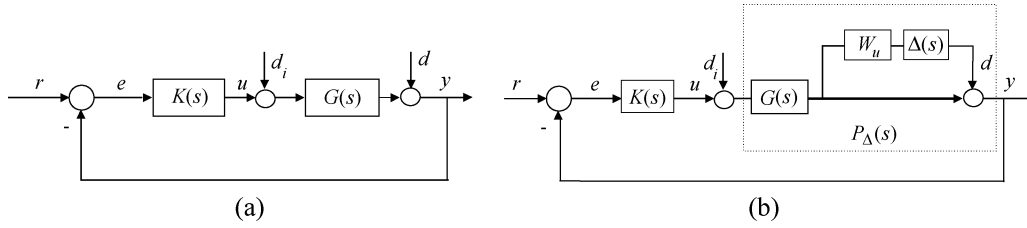
Fig. 1. (a) Typical diagram of a feedback control system and (b) multiplicative unstructured uncertainty description.

where $\bar{\sigma}(S(j\omega))$ is the maximum singular value of $S(j\omega)$, and W_1 is a bound on $\bar{\sigma}(S(j\omega))$ which reflects the desired disturbance attenuation for each frequency ω. Thus, good disturbance rejection would require the satisfaction of (2), particularly in the low-frequency range, where d and d_i are usually significant. If $\underline{\sigma}(GK) \gg 1$, then $S \approx (GK)^{-1}$, and from (2) one obtains $\underline{\sigma}(GK) \geq |W_1|$ with $\underline{\sigma}(GK)$ the minimum singular value which can be defined in terms of the maximum singular value of the inverse of the matrix GK by $\bar{\sigma}((GK)^{-1}) = 1/\underline{\sigma}(GK)$. The transfer function from input r to control u is given by $R(s) = K(s)S(s)$. Hence, a constraint on the control u can be introduced with a bound on $\bar{\sigma}(K(j\omega)S(j\omega))$ specified by

$$\bar{\sigma}(K(j\omega)S(j\omega)) \leq \left| W_2^{-1}(j\omega) \right| \qquad (3)$$

where $W_2(j\omega)$ is a weighing function to be specified.

A. Perturbation Model

Physical systems typically undergo a variety of perturbations. Uncertainty in the mathematical model of the system is, in general, described as a perturbation to the nominal system. The uncertainty is termed unstructured when it is only known in terms of upper and lower bounds and structured when its detailed model is known. For a set of perturbations $\Delta(s)$ satisfying the infinity norm $\|\Delta\|_\infty \leq 1$, the perturbed plant may be modeled in terms of a multiplicative unstructured uncertainty, in respect to the nominal plant G, as follows:

$$P_\Delta = (I + \Delta_M)G, \quad \Delta_M = W_u\Delta \qquad (4)$$

with W_u stable transfer functions that characterize the frequency structure of the uncertainty. Fig. 1(b) illustrates this uncertainty modeling approach. Practical engineering systems, in general, operate under perturbations so that a closed-loop stability robustness test is needed [7]. This test should indicate the worse case operation associated with typical modeled perturbations. If the system in Fig. 1(b) with $\Delta = 0$ is stable, the size of the smallest stable $\Delta_M(s)$ for which the system becomes unstable is thus given by

$$\bar{\sigma}(\Delta_M(j\omega)) = \frac{1}{\bar{\sigma}(T(j\omega))}. \qquad (5)$$

The result on stability robustness (5) is given in terms of the singular values of the multiplicative perturbation and complementary sensitivity matrices [8]. A smaller $\bar{\sigma}(T(j\omega))$ corresponds

to a larger minimum for the destabilizing multiplicative uncertainty and hence to a larger stability margin. As a consequence, usually an upper bound on $\|T(s)\|$ is specified as follows:

$$\bar{\sigma}(T(j\omega)) \leq \left| W_3^{-1}(j\omega) \right| \qquad (6)$$

where W_3 is a weighting function used to tailor the system stability condition. Thus, good robustness and noise rejection would require the satisfaction of (6), particularly in the high-frequency range where the noise and modeling errors are usually significant. If $\bar{\sigma}(GK) \ll 1$ then $T \approx GK$, and from (6) one obtains $\bar{\sigma}(GK) \leq |W_3^{-1}|$.

The understanding of the effects of the weighting functions on the control system is crucial for modeling the desired specifications. From Figs. 1(a) and (2), (3), and (6), a typical interconnection model for design is illustrated in Fig. 2(a), wherein, the weighting functions W_1, W_2, and W_3 reflect the steady-state specified error and the disturbance attenuation, controller input constraints and stability condition, respectively, in the following way:

1) W_1 weights the system sensitivity S reflecting the performance specifications;
2) W_2 weights KS reflecting the control input constraints;
3) W_3 weights the complementary sensitivity T and tailors the stability condition.

In Fig. 2, $P(s)$ defines an augmented plant with w and u inputs and z and y outputs. The output z is the vector of regulated variables. Here, w and y correspond to the reference command r and error e of the typical feedback diagram of Fig. 1(a), respectively. The input–output mapping of the system in Fig. 2 is described by

$$\begin{bmatrix} z \\ y \end{bmatrix} = P \begin{bmatrix} w \\ u \end{bmatrix} = \begin{bmatrix} P_{11} & P_{12} \\ P_{21} & P_{22} \end{bmatrix} \begin{bmatrix} w \\ u \end{bmatrix}, \qquad (7)$$

$$u = K(s)y. \qquad (8)$$

Substituting $u = K(s)y$ in (7), the closed-loop transfer matrix from w to z can be found as

$$T_{zw} = P_{11} + P_{12}K(I - P_{22}K)^{-1}P_{21}. \qquad (9)$$

In the literature, the mapping in (9) is called an LFT. The notation usual for an LFT is $\mathcal{F}_\ell(P, K)$, with the superscript "ℓ" denoting lower LFT. This designation is associated to the position of the feedback loop in respect to the direct loop in the two-block structure of the system.
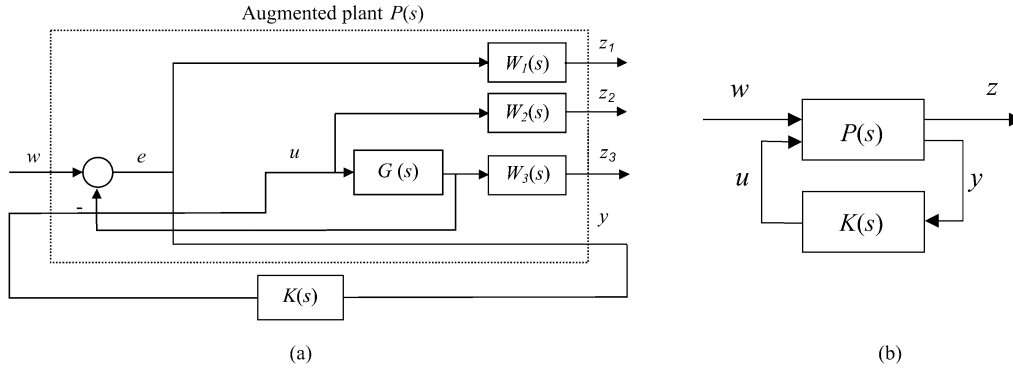
Fig. 2.   (a) Augmented plant with weighting functions and (b) simplified two-block diagram.
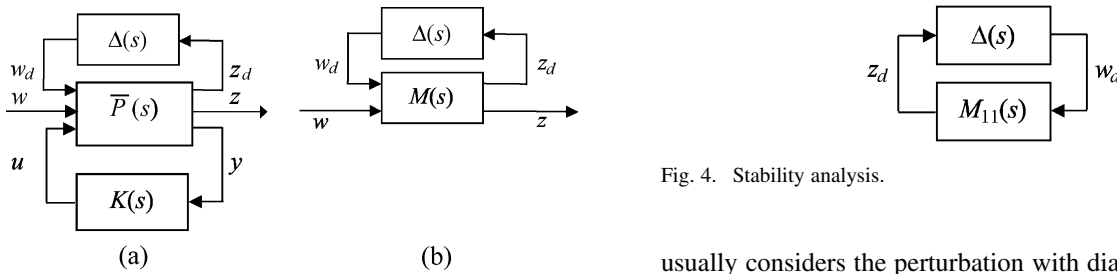

Fig. 3.   General block and $M - \Delta$ structures.

III. μ ANALYSIS AND SYNTHESIS

In this section, an overview of the main results on robustness analysis and μ design, including the key concepts and interpretations to facilitate the understanding of the main tools available, are presented.

A. General Control Design Structure

To model general systems, one should consider the connected system in a three-block structure form shown in Fig. 3(a), wherein an uncertainty block Δ is included. Using the LFT $\mathcal{F}_\ell(\bar{P}(s), K(s))$, the connected system in the three-block form can be reduced to the $M - \Delta$ two-block structure shown in Fig. 3(b), which can be described as follows:

$$
\begin{bmatrix} z_d \\ z \end{bmatrix} = M \begin{bmatrix} w_d \\ w \end{bmatrix} = \begin{bmatrix} M_{11} & M_{12} \\ M_{21} & M_{22} \end{bmatrix} \begin{bmatrix} w_d \\ w \end{bmatrix}
$$
$$
w_d = \Delta z_d
$$
$$
z = \mathcal{F}_u(M, \Delta) w = \left[M_{22} + M_{21}\Delta(I - M_{11}\Delta)^{-1} M_{12} \right] w \tag{10}
$$

where the superscript "u" denotes upper LFT. From (10) the transfer matrix from the output vector z to reference or disturbance w is obtained as $T_{zw} = \mathcal{F}_u(M, \Delta)$. The mapping $\bar{P}$ in Fig. 3 differs from mapping P in Fig. 2 in the number of inputs and outputs since input w_d and output z_d are added to model the system perturbation.

For more general perturbation descriptions, the analysis for the robustness problem can be formulated in a unified framework using LFT and the structured singular value (SSV). One

usually considers the perturbation with diagonal and block-diagonal terms

$$
\Delta = \{ \operatorname{diag}\left[\delta_1 I_{r_1}, \ldots, \delta_s I_{r_S}, \Delta_1, \ldots, \Delta_F \right] :
$$
$$
\delta_i \in \mathbb{C}, \Delta_j \in \mathbb{C}^{m_j \times m_j} \}
$$

where subscripts S and F are the number of scalar and full blocks, respectively. A norm-bounded subset of Δ is defined as $\mathbf{B}\Delta = \{ \Delta \in \Delta : \bar{\sigma}(\Delta) \leq 1 \}$.

B. Stability Robustness

The stability of a system subject to perturbation Δ is determined by analyzing the feedback system in Fig. 3(b). Assuming the nominal feedback system stable, any unstable poles are the solutions of

$$
\det\left(I - M_{11}(s)\Delta(s) \right) = 0. \tag{11}
$$

Stability robustness is evaluated by the smallest destabilizing perturbation Δ that results in a solution of (11) on the imaginary axis. The smallest perturbation Δ is defined in terms of $\bar{\sigma}(\Delta)$ as follows:

$$
\inf_w \left\{ \min_{\Delta \in \mathbf{B}\Delta} \left[\bar{\sigma}(\Delta) \text{ such that } \det(I - M_{11}\Delta) = 0 \right] \right\}.
$$

A measure of the smallest destabilizing perturbation Δ is given in terms of the SSV and is denoted μ_Δ. The μ measure can be seen as a stability margin with respect to the uncertainty Δ. A formal definition can be found in [7].

The well-known small-gain theorem establishes that for $M(s)$ internally stable and for all admissible perturbations $\Delta \in \mathbf{B}\Delta$, the feedback system in Fig. 3 is internally stable if, and only if, $\sup_\omega \mu_\Delta(M_{11}(j\omega)) < 1$ [9]. As $M(s)$ is stable, the instability can only be caused by the perturbation Δ so that the analysis of stability can be carried out with Fig. 4.

Fig. 4.   Stability analysis.

C. Performance Robustness

Stability is the basic requirement of closed-loop control systems, but suitability of the controller is also dependent on the meeting of the specified performance. For the typical interconnection model shown in Fig. 2, the transfer matrix from z to w denoted T_{zw} is obtained as follows:

$$T_{zw} = [W_1 S \ W_2 KS \ W_3 T]^T. \qquad (12)$$

From (2), (3), and (6), one can easily see that the performance specifications can be described using upper bounds given in terms of singular values of the transfer matrices in (12). Therefore, one usually specifies the design requirements in terms of the infinity norm

$$\|T_{zw}\|_\infty < 1. \qquad (13)$$

In (13), the motivation to call the transfer matrix of interest T_{zw} is the connection between robust control and the disturbance attenuation problem in which w stands for the disturbance inputs. A robustness performance condition guarantees the system performance specifications for all admissible perturbations. A feedback system meets performance robustness if the system is kept internally stable and condition (13) is satisfied for all admissible perturbations. From the small-gain theorem and condition (13), performance robustness conditions are thus established as follows:

$$\sup_\omega \mu_\Delta (M_{11}(j\omega)) < 1, \qquad (14)$$

$$\|T_{zw}\|_\infty < 1. \qquad (15)$$

The robust performance problem can be formulated as an equivalent robust stability problem by appending a virtual uncertainty block to the augmented plant. This uncertainty block connects the performance output to the augmented plant input. An important result for robustness analysis that relates performance specifications and stability is given next.

Let the virtual perturbation block be Δ_f, and let M be a stable transfer function. Also, let $w \in \mathcal{R}^{q_2}$ and $z \in \mathcal{R}^{p_2}$. Thus, the augmented uncertainty structure is as follows:

$$\Delta_P = \left\{ \begin{bmatrix} \Delta & 0 \\ 0 & \Delta_f \end{bmatrix} : \Delta \in \mathbf{B\Delta}, \Delta_f \in \mathbb{C}^{q_2 \times p_2} \right. \qquad (16)$$

with $\|\Delta_f\|_\infty \leq 1$.

The system in Fig. 5 meets the robustness conditions (14) and (15) if, and only if, it is internally stable [9]. This result on robust performance is crucial to understand why the performance criterion is established in the same way as the stability criterion given by the small-gain theorem. The analysis of stability and performance margins are called μ analysis. A complete text in robust control theory can be found, for example, in [7] and [10]. In the latter, MATLAB functions for robust control are also indicated.

D. μ Design

The control design objective is to find a stabilizing controller K so that for all perturbations $\Delta \in \mathbf{B\Delta}$, the feedback system is stable and satisfies $\|\mathcal{F}_\ell[\mathcal{F}_u(\bar{P},\Delta),K]\|_\infty < 1$, and the μ synthesis goal is to minimize the peak of $\mu_\Delta(.)$ of the feedback
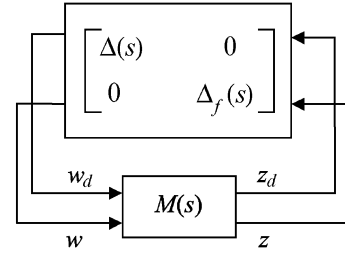

Fig. 5. LFT of the augmented perturbation system.

transfer function $\mathcal{F}_\ell(\bar{P},K)$ over all the stabilizing controllers K

$$\min_{\substack{K \\ \text{stabilizing}}} \ \max_w \mu_\Delta \left(\mathcal{F}_\ell(\bar{P},K)(jw) \right). \qquad (17)$$

In the min–max problem (17), reducing the upper bound on μ_Δ allows an increase in the smallest destabilizing perturbation Δ, thus increasing the robustness stability margin. The direct computation of $\mu_\Delta(M)$ by a search over all $\Delta \in \mathbf{B\Delta}$ is not tractable. Therefore, an upper bound on $\mu_\Delta(M)$ is used in the design of robust controllers. An upper bound on $\mu_\Delta(M)$ is $\bar{\sigma}(M)$. However, this upper bound tends to be conservative. To overcome this problem, a concept of diagonal scaling to compute the upper bounds on μ_Δ was introduced in [11]. The motivation for this approach is that if Δ and D are diagonal matrices, $\|\Delta\|_\infty = \|D\Delta D^{-1}\|_\infty$ but $\|DMD^{-1}\|_\infty$ can be made much smaller than $\|M\|_\infty$. Therefore, as the nominal closed-loop poles of the system in Fig. 3(b) are not affected by a diagonal scaling, it follows that

$$\mu_\Delta(M) = \mu_\Delta(DMD^{-1}). \qquad (18)$$

This result leads to the following upper bound for $\mu_\Delta(M)$ where

$$\mu_\Delta(M) \leq \inf_{D \in \mathcal{D}} \bar{\sigma}(DMD^{-1}) \qquad (19)$$

with $\mathcal{D}$ a set of scaling diagonal matrices with the property $D\Delta = \Delta D$ for every $D \in \mathcal{D}$ and $\Delta \in \Delta \in \mathbf{B\Delta}$.

The minimizing problem (17) can be solved iteratively for K and D. This procedure is called $D - K$ iteration. For a chosen D, the minimizing problem can be established as

$$\min_{\substack{K \\ \text{stabilizing}}} \ \min_{D,D^{-1} \in H_\infty} \left\| D\mathcal{F}_\ell(\bar{P},K)D^{-1} \right\|_\infty \qquad (20)$$

where H_∞ denotes the subspace of stable transfer matrices.

Algorithm 1 ($D - K$ Iteration)

1) Establish an initial estimative of the scaling matrix $D_\omega = diag(d_1^\omega I, \ldots, d_{F-1}^\omega I, I) \in \mathcal{D}$, d_i^ω, $i = 1, \ldots, F-1$ positive scalars.
2) Find stable scalar transfer functions $d_i(s)$, $d_i^{-1}(s)$ for $i = 1, 2, \ldots, F-1$ so that $|d_i(j\omega)| \approx d_i^\omega$.
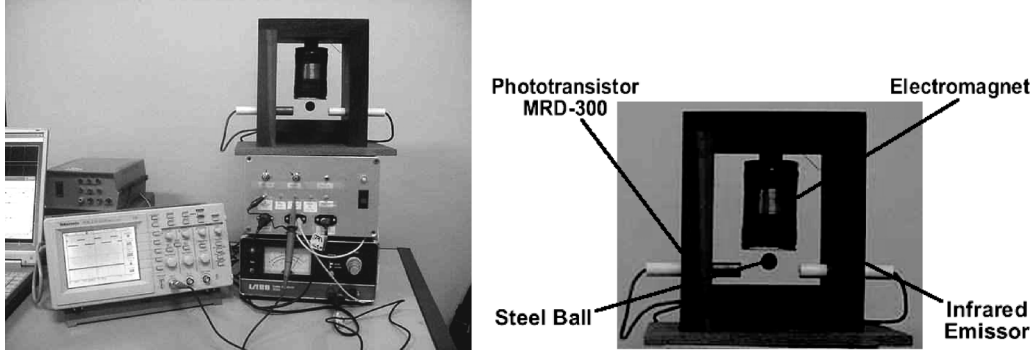3) Let $D(s) = diag(d_1(s)I, \ldots, d_{F-1}(s)I, I)$.

Fig. 6. Experimental setup and maglev device.

4) Construct a space state model for system $\hat{P} = D(s)\bar{P}D^{-1}(s)$.
5) Solve the H_∞ optimization problem $\min_K \|\mathcal{F}_\ell(\hat{P}, K)\|_\infty$ and denote the controller found by $\hat{K}$.
6) Solve

$$\min_{D_\omega \in \mathcal{D}} \bar{\sigma}\left[D_\omega \mathcal{F}_\ell(\bar{P}, \hat{K})(j\omega)D_\omega\right] \qquad (21)$$

and denote the new D_ω by $\hat{D}_\omega$.
7) Compare $\hat{D}_\omega$ with the previous estimate D_ω and return to Step 2) until convergence is reached.

IV. SYSTEM EQUATIONS

In this section, the maglev device and components are described. The nonlinear equations are first presented to call attention to a linear control design developed for a nonlinear plant. The maglev device used is illustrated in Fig. 6, which is composed of an electromagnet, a position detector, and a power amplifier working with an analog pulsewidth modulation (PWM) circuit of 5-kHz switching frequency and a transistorized dc chopper. The position detector consists of a 5-V infrared emissor and a phototransistor MRD-300 receptor. The objective of the control design is to keep the ball in a dynamic balance around a desired operation point. The modeling of the maglev system is based on its electrical, mechanical, and electromechanical equations [12], [13]

$$f(h,i) = \frac{-L_0}{2a}\frac{i^2}{(1+h/a)^2}$$
$$m\frac{d^2h}{dt^2} = mg + f(h,i)$$
$$k_a v = Ri + \frac{d\left(L(h)i\right)}{dt} \qquad (22)$$

where $f(.,.)$ is the electromagnetic force; i is the coil current; h is the ball position; v is the applied voltage; $L(.)$ and R are coil inductance and resistance, respectively; a is a constant; $L_0 = L(0) - L(\infty)$; and k_a is the power amplifier gain. Let the maglev system state variables be $x_1 = h$, $x_2 = \dot{h}$, $x_3 = i$, and output y the sensor output. Thus, using (22), one obtains

$$\dot{x} = F(x) + Bv, \quad y = Cx \qquad (23)$$

where

$$F(x) = \begin{bmatrix} x_2 \\ g - \left(\frac{L_0}{2am}\right)\left(\frac{x_3}{1+(x_1)/a}\right)^2 \\ -\frac{R}{L}x_3 \end{bmatrix}, \quad B = \begin{bmatrix} 0 \\ 0 \\ k_a/L \end{bmatrix},$$
$$C = \begin{bmatrix} c_1 & 0 & 0 \end{bmatrix}$$

with c_1 the position sensor gain and L a constant which approximates $L(.)$ in the vicinity of z_0. Now, linearizing (23) using the first-order Taylor's expansion around the equilibrium (h_0, i_0) for $x_\ell = [h - h_0 \; \dot{h} \; i - i_0]^T$ and $u = v - (Ri_0/k_a)$, one obtains

$$\dot{x}_\ell = Ax_\ell + Bu, \quad y = Cx_\ell \qquad (24)$$

where

$$A = \begin{bmatrix} 0 & 1 & 0 \\ k_2/m & 0 & -k_1/m \\ 0 & 0 & -R/L \end{bmatrix}$$

with

$$k_1 := \left.\frac{\partial f}{\partial i}\right|_{(h_0,i_0)} = \frac{L_0 i_0}{[a(1+h_0/a)^2]}$$
$$k_2 := \left.\frac{\partial f}{\partial h}\right|_{(h_0,i_0)} = \frac{L_0 i_0^2}{[a^2(1+h_0/a)^3]}. \qquad (25)$$

The nominal linearized model of the maglev system described above is used in the control design with $L = 0.52$ H, $R = 21$ Ω, $k_a = 2.1$ V/V, $c_1 = -1.7361 \times 10^3$ V/m, $h_0 = 0.0045$ m, $i_0 = 0.5773$A, $L_0 = 24.9 \times 10^{-3}$ H, $a = 6.72 \times 10^{-3}$ m, and $m = 0.00226$ Kg. In the equilibrium (h_0, i_0), one obtains $mg = -f(h_0, i_0)$. Here, one can recall the first method of Lyapunov to analyze the stability of the equilibrium from the linearized model (24).

V. DESIGN PROCEDURE

A. Parameter Uncertainty

Motivated by the use of magnetic systems in transportation systems [14], the mass is subjected to variations. For a deviation of 10% in the steel ball mass m, one can write $m = \bar{m} + 0.1\delta\bar{m}$, $-1 \leq \delta \leq 1$ with m the real mass and $\bar{m}$ the nominal mass. This

mass perturbation is described in the augmented plant shown in Fig. 8 by a LFT in δ. In fact, the term $1/m$ can be written as

$$\frac{1}{m} = \frac{1}{\bar{m}} - \frac{0.1\delta}{\bar{m}}(1 + 0.1\delta)^{-1}. \qquad (26)$$

Comparing (10) and (26), the corresponding LFT matrix denoted M_1 can be found as

$$M_1 = \begin{bmatrix} -0.1 & 1 \\ \frac{-0.1}{\bar{m}} & \frac{1}{\bar{m}} \end{bmatrix}. \qquad (27)$$

The LFT can be represented in the form

$$\frac{1}{m + 0.1\delta} \Leftrightarrow \mathcal{F}_u\left(\delta, \begin{bmatrix} -0.1 & 1 \\ -\frac{0.1}{\bar{m}} & \frac{1}{\bar{m}} \end{bmatrix}\right).$$

B. Weighting Functions

The selection of the weighting functions for a specific design problem is, in general, an involved task. The guidelines used to choose the weighting functions W_1, W_2, and W_3 for the maglev system are summarized below.

The function W_1 is bound for the sensitivity function S and reflects external disturbance rejection, a small steady-state error with respect to the desired equilibrium, and plant variations tolerance. Considering that the bandwidth of the maglev system ranges from 10 to 100 rad/s, to achieve a small steady-state error an integral term approximated by a pole at $s = 0.1$ is included in W_1. Now, the gain is set to 22.5 to achieve a steady-state gain between the desired equilibrium and the error less than -20 dB, thus yielding

$$W_1 = \frac{2.25}{s + 0.1}. \qquad (28)$$

The function W_3 is selected so that a peak requirement on the complementary sensitivity function T is satisfied to reduce the system oscillations and to limit T in the high-frequency range for stability. However, these requirements are in conflict with W_1. After simulation and fine tuning, the cutoff frequency of W_3 is set to 190 rad/s (above the closed-loop bandwidth frequency), and its zero set to 20 rad/s so that the peak on T is reduced, thus yielding

$$W_3 = \frac{0.075(s + 20)}{s + 190}. \qquad (29)$$

Finally, the function W_2 should have a sufficiently large gain to constraint the control input to an acceptable range to avoid the saturation of the actuator. However, since a large gain can deteriorate the system performance, a tradeoff must be sought with the function W_2 set so that the high-frequency noises are attenuated as much as possible, and the speed of the system response is
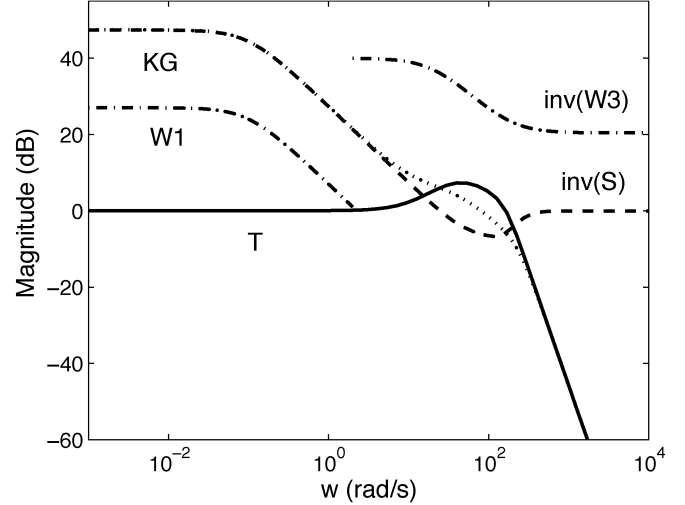

Fig. 7. Specification requirements.

kept acceptable. Considering that the actuator input cannot exceed 10 V, after simulation and fine tuning, the weighting function W_2 is chosen as

$$W_2 = \frac{0.0045(s + 20)}{s + 150}. \qquad (30)$$

C. Standard H_∞ Controller

The standard H_∞ control problem is formulated in terms of finding an admissible controller K, if there is one, so that, for a given $\gamma > 0$

$$\|T_{zw}\|_\infty := \left\|[W_1 S \; W_2 K S \; W_3 T]^T\right\|_\infty \le \gamma. \qquad (31)$$

The framework of H_∞ control is very flexible and can include performance specifications, disturbance rejection, control input limitations, and robustness requirements. To model the performance and stability requirements, an augmented plant is obtained from the nominal plant G and weighting functions. To consider a perturbed model for the plant in terms of a multiplicative uncertainty which reflects a variation in the mass m, a stable transfer function W_u generated from (4) is used to adjust the weighting function W_3. Therefore, the stability condition for the multiplicative uncertainty $\|W_u T\|_\infty < 1$ is also guaranteed, and W_3 is altered to

$$W_3 = \frac{0.095s + 1.9}{s + 190}. \qquad (32)$$

The augmented plant used follows the structure shown in Fig. 2 and is obtained with the function `augtf`

```
[tss_] = augtf(G, W1, W2, W3);
                    /* builds the augmented plant */
```
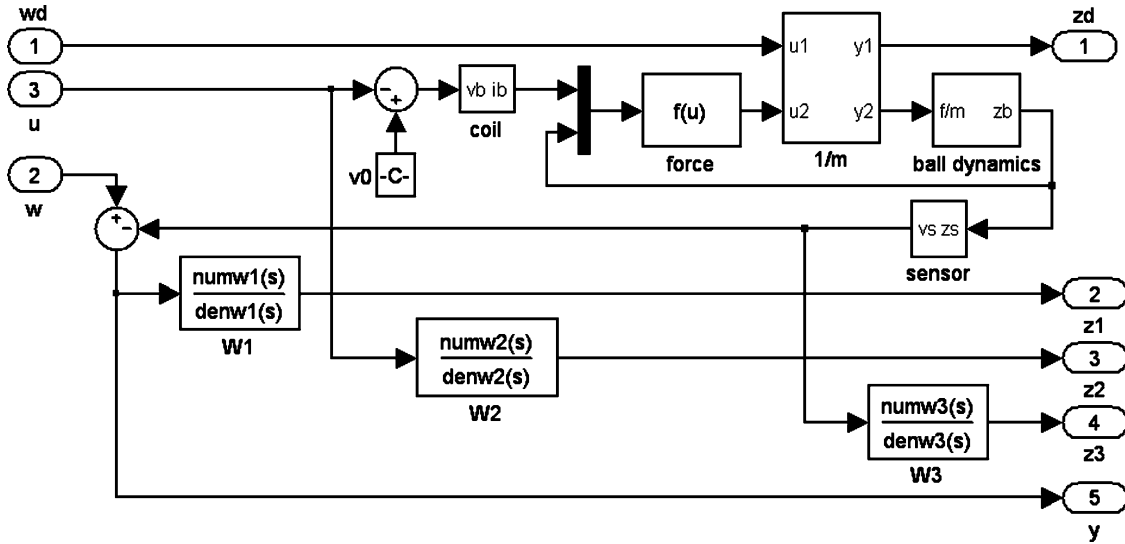
Fig. 8. Simulink block diagram to obtain the augmented P (Pmu.mdl).

and the H_∞ controller is thus obtained via the following functions:

$[\mathrm{ss\_cp}, \mathrm{ss\_cl}] = \mathrm{hinf}(\mathrm{tss\_});$
  $/ * \mathrm{solves\ the\ H - infinity\ problem} * /$ and
$[\mathrm{syscc}] = \mathrm{ss}(\mathrm{ss\_cp});$
  $/ * \mathrm{obtains\ the\ controller\ space - state\ form} * /$

where $\mathrm{ss\_cp} = \mathrm{mksys}(\mathrm{Ac}, \mathrm{Bc}, \mathrm{Cc}, \mathrm{Dc})$ with Ac, Bc, Cc, Dc the matrices of the controller found and $\mathrm{ss\_cl}$ the corresponding closed-loop system. The controller found is of order 6. The function "hinf" uses a two-Riccati algorithm [7]. Fig. 7 illustrates the performance and stability bounds specified in terms of W_1 and W_3^{-1} as in (2) and (6).

D. μ Controller

The same weighting functions used in the standard H_∞ controller are used in the design of the μ controller. The uncertainty is described in terms of an LFT augmented with the addition of an input and output. The matrix $\bar{P}$ for the control problem modeling as in Fig. 8 describes the connected system $[z_d z_1 z_2 z_3 y]^T = \bar{P}[w_d\ w\ u]^T$.

The solution of (20) provides the minimization of $\|W_1 S\|_\infty$, $\|W_2 K S\|_\infty$, $\|W_3 T\|_\infty$, and $\sup_\omega \mu_\Delta (M_{11}(j\omega)) < 1$ by the small-gain theorem and the robust performance conditions. The μ synthesis controller can be obtained with MATLAB using the following functions [15]:

$[\mathrm{Ap}, \mathrm{Bp}, \mathrm{Cp}, \mathrm{Dp}] = \mathrm{linmod}(`\mathrm{Pmu}');$
  $/ * \mathrm{obtains\ augmented\ plant}\ \bar{P}\ \mathrm{from}\ `\mathrm{Pmu}' * /$
$\bar{P} = \mathrm{pck}[\mathrm{Ap}, \mathrm{Bp}, \mathrm{Cp}, \mathrm{Dp}];$
  $/ * \mathrm{packs\ state - space\ data\ into}$
    $\mathrm{system\ matrix\ form} * /$
$\mathrm{dk\_def\_name} = `\mathrm{G\_dk.m}';$
  $/ * \mathrm{defines\ name\ for\ the\ D - K\ file} * /$
$\mathrm{dkit};\ / * \mathrm{implements\ mu - synthesis\ iteration} * /$

The file G_dk.m must contain

$\mathrm{nominal\_dk} = \bar{P};\ / * \mathrm{connected\ plant\ structure} * /$
  $\mathrm{nmeas\_dk} = 1;\ / * \mathrm{number\ of\ outputs} * /$
  $\mathrm{ncont\_dk} = 1;\ / * \mathrm{number\ of\ control\ inputs} * /$
    $\mathrm{blk\_dk} = [-1\ 0;\ 1\ 3];$
      $/ * \Delta\ \mathrm{structure\ to\ calculate}\ \mu_\Delta * /$
  $\mathrm{omega\_dk} = \mathrm{logspace}(-1, 4, 200);$
      $/ * \mathrm{frequency\ range\ of\ responses} * /$

E. μ Analysis

A sixth-order controller K with the smallest peak μ_{Δ_P} is found in the seventh $D - K$ iteration for an order zero scaling matrix D. The μ analysis of the feedback system is carried out with the following commands:

$\mathrm{M} = \mathrm{starp}(\bar{P}, \mathrm{K}, 1, 1);$
  $/ * \mathrm{obtains\ Redheffer\ star - product\ of}\ \bar{P}\ \mathrm{and\ K} * /$
$\mathrm{M\_f} = \mathrm{frsp}(\mathrm{M}, \mathrm{omega\_dk});$
  $/ * \mathrm{obtains\ complex\ frequency\ response} * /$
$[\mathrm{bnds}] = \mathrm{mu}(\mathrm{M\_f}, [-1\ 0;\ 1\ 3]);$
  $/ * \mathrm{obtains}\ \mu_{\Delta_p}(M)\ \mathrm{for\ performance}$
    $\mathrm{robustness\ test} * /$
$\mathrm{M11} = \mathrm{sel}(\mathrm{M}, 1, 1);$
  $/ * \mathrm{selects\ block\ M11\ from\ M\ to\ analyse\ the}$
    $\mathrm{feedback\ system\ in\ Fig.\ 4} * /$
$[\mathrm{AM11}, \mathrm{BM11}, \mathrm{CM11}, \mathrm{DM11}] = \mathrm{unpck}(\mathrm{M11})$
  $/ * \mathrm{obtains\ space - state\ form\ of\ M11} / *$
$[\mathrm{mu}, \mathrm{LOGD}] = \mathrm{SSV}(\mathrm{AM11}, \mathrm{BM11}, \mathrm{CM11}, \mathrm{DM11}, \mathrm{w}, [-1\ -1]);$
  $/ * \mathrm{obtains}\ \mu_\Delta(M_{11})\ \mathrm{for\ stability\ test} * /$

where input $[-1\ 0; 1\ 3]$ is the size of the uncertainty and fictitious uncertainty blocks and output LOGD gives the optimal diagonal scaling D for M_{11}.
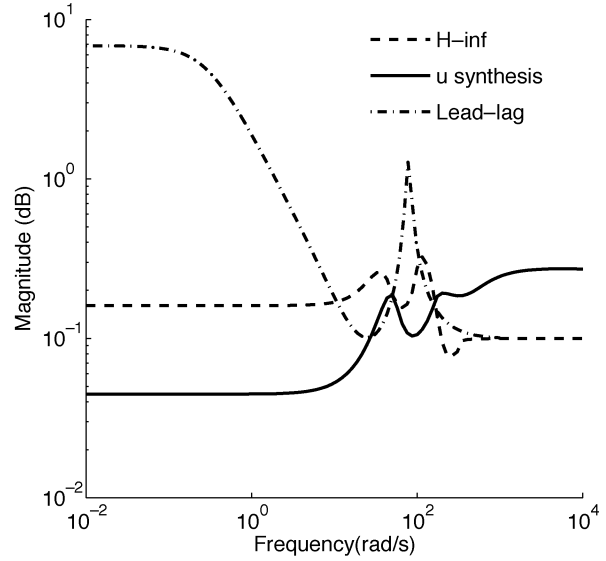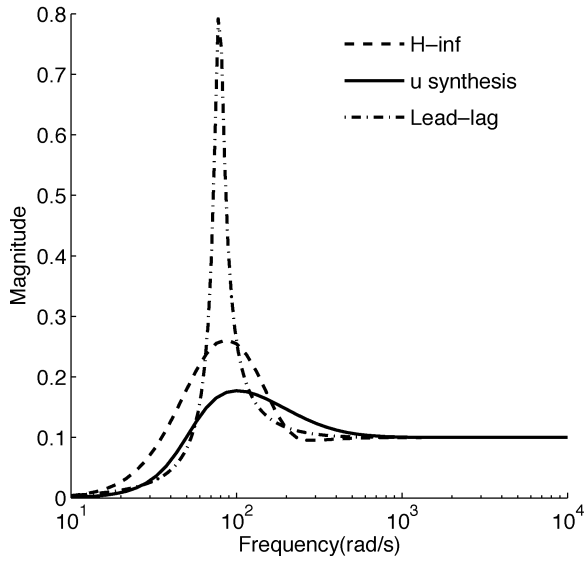
Fig. 9. Robust stability test (left) and robust performance test (right) for the three controllers.

The frequency response for the stability test is shown in Fig. 9 (left), which presents the obtained upper bound for μ. The peak value occurs about 100 radians/second which is the most critical system frequency. The peak value of μ are 0.79, 0.261, and 0.177 for the lead–lag, H_∞, and μ controllers, respectively. These bounds indicate the corresponding intervals of m for robust stability, which are $0.875\bar{m} < m < 1.125\bar{m}$, $0.615\bar{m} < m < 1.380\bar{m}$, and $0.435\bar{m} < m < 1.565\bar{m}$, respectively.

The frequency response for robust performance is shown in Fig. 9 (right). This result shows that the uncertainty in the mass m deteriorates the performance about the frequency 100 rad/s. However, the solutions given by the H_∞ and μ controllers achieve robust performance to uncertainty in the mass for $0.692\bar{m} \leq m \leq 1.308\bar{m}$ and $0.633\bar{m} \leq m \leq 1.366\bar{m}$. The peak values of μ found in this case are 6.84, 0.325, and 0.273 for the lead–lag, H_∞, and μ controllers, respectively.

The maglev system could be stabilized with a lead controller. However, to reduce the position steady-state error, a second-order lead–lag controller is used in the comparisons. The lead–lag is found with the function sisotool of MATLAB, which is a graphical user interface to design single-input/single-output (SISO) compensators by simultaneously interacting with the root locus and Bode diagrams of the open-loop system and the output and control responses of the feedback system. After several trials in the sisotool, the transfer function of the controller found is

$$K_{\text{lead}-\text{lag}}(s) = \frac{17.6s^2 + 315.1s + 62.22}{s^2 + 490s + 49} \qquad (33)$$

and the discrete state-space form for controller (33) is found using

```
[Ac, Bc, Cc, Dc] = tf2ss(numK, denK);
        /* obtains the space-state
           form of the controller */      .
[Ad, Bd, Cd, Dd] = BILIN(Ac, Bc, Cc, Dc, 1, 'Tustin', 0.001)
        /* performs bilinear transform */
```

Fig. 10 shows the Simulink diagram employed to obtain the simulation results of the system under perturbations using the nonlinear model of the maglev system. The results obtained with the linearized model may present significant discrepancies. These discrepancies may add more involved tuning in the selection of the weighting functions if the initial conditions are not taken closer to the operating point (h_0, i_0).

VI. CLASS ASSIGNMENTS

The main difficulty encountered in teaching control is the variety of concepts involved in a single control lecture since the student has to integrate concepts from linear algebra, differential equations, and dynamic systems. Each class period has about 50 minutes of lecture followed by 50 minutes of simulation studies. To motivate the students on the topics being taught, one or two students at a time are assigned homework. In the following week, these students introduce in class their homework solutions which are then given to the others as oriented class work. To facilitate the completion of the homework, further instructions are given to them during the week. To use robust control design in practical problems, one finds that the concepts of augmented plant, performance specification, and weighing functions and interconnected models are of paramount importance. Some possible work class tasks involving these concepts include the following.

1) *Analysis and synthesis*:
   a) analysis of the stability of the equilibrium (h_0, i_0) of the nonlinear equations using a linearization model with the system parameter values given in Section IV;
   b) description of the perturbed plant and choice of weighting functions following the guide lines given in Section V-A and V-B;
   c) construction of the augmented plant in Figs. 2 and 8 for design using the procedure provided in Section V-C and V-D, respectively.
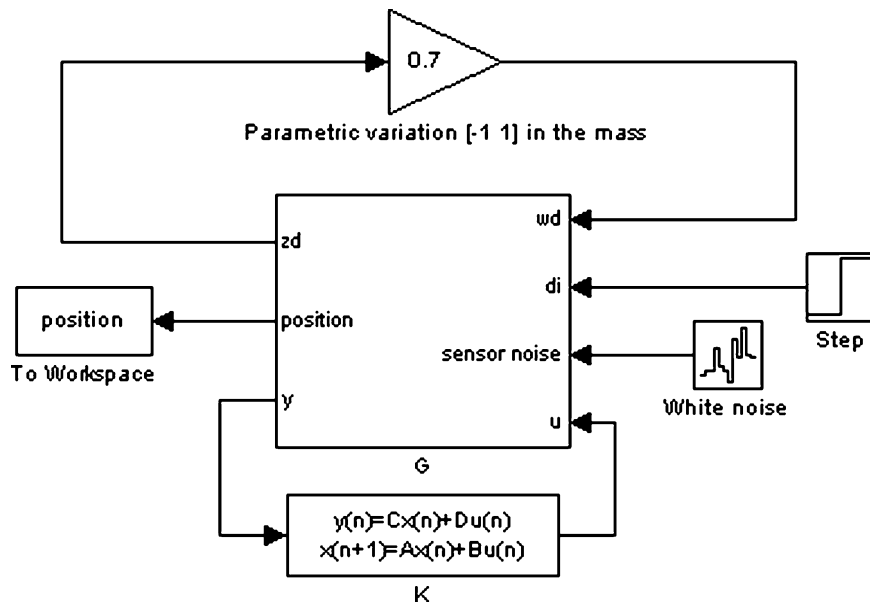
Fig. 10.   Simulink model for the controlled plant under perturbations.

d) development of a MATLAB program to obtain the standard H_∞ and μ controllers using the steps provided in Sections V-C and V-D, respectively; for the purpose of comparison a lead–lag controller can be found with the MATLAB function sisotool;

e) development of a MATLAB program to perform the robustness tests in terms of the upper bounds on μ using the steps given in Section V-E; typical plots obtained by the students are shown in Fig. 9.

At this point, the students should get the feeling that higher order lead–lag controllers would provide better solutions than the second order obtained. The drawback is that these solutions would not be found via a systematic procedure, such as the case of the robust controller designs studied.

2) *Simulation work*:

a) develop a Simulink diagram of the type showed in Fig. 10 to obtain responses to a disturbance step;

b) plot the feedback system responses for the lead-lag controller obtained; typical plots obtained by the students are shown in Fig. 16;

c) repeat for different amplitudes of the disturbance and variation of the mass for the standard H_∞ and μ controllers obtained; typical plots obtained by the students are shown in Figs. 17 and 18.

3) *Final course project*:

A project is sought to relate analysis and synthesis. The project should be on successful applications of control found in the literature. For this task, the students are divided into small groups and required to develop the design and simulation tests related to the application chosen. The control problem formulation, the main robustness tests, and simulation results obtained by each group are then presented in class, taking about 15 minutes. This step has a good impact on the participation of the students in class discussions favoring the understanding of control techniques. The laboratory experiment presented next use

the maglev device described before and may serve as a project for a group of students. The students' presentation should include a description of the computational platform used, control system components, discretization of the controller, and the main advantages and disadvantages of the obtained controllers.

VII. LABORATORY EXPERIMENT

A. Controller Discretization

The solution of the robust design techniques used is a high order continuous controller. To obtain the controller discrete space state description from its continuous space state form, the Tustin's rule is used since it yields satisfactory results for high order systems when the sampling time is chosen appropriately. This transformation is also called a bilinear transformation because of its mathematical form. To recover the bandlimited continuous signal from the sampled signal, one can recall the Shannon's sampling theorem which establishes that $\omega_0 > 2\omega_{max}$ with ω_{max} the maximum frequency of the continuous signal and ω_0 the sampling frequency. The Shannon frequency plays an important role as a reference frequency since continuous signals are not in general bandlimited. The sampling frequency is thus chosen as 1 kHz to provide an accurate bilinear transformation in the system bandwidth.

The block diagram realization of the discrete state space controller is implemented via shift registers elements, adders, and multipliers using the usual block diagram description. The software LabVIEW is used to implement the digital controller. LabVIEW is a development platform that uses a graphical programming language relying on icons and graphical symbols to specify programming tasks. The environment of LabBVIEW consists of a front panel and a block diagram. A sequence structure of two subdiagrams which are executed sequentially with the variables control signal and ball position passed to the second subdiagram to be saved in a file for further analysis
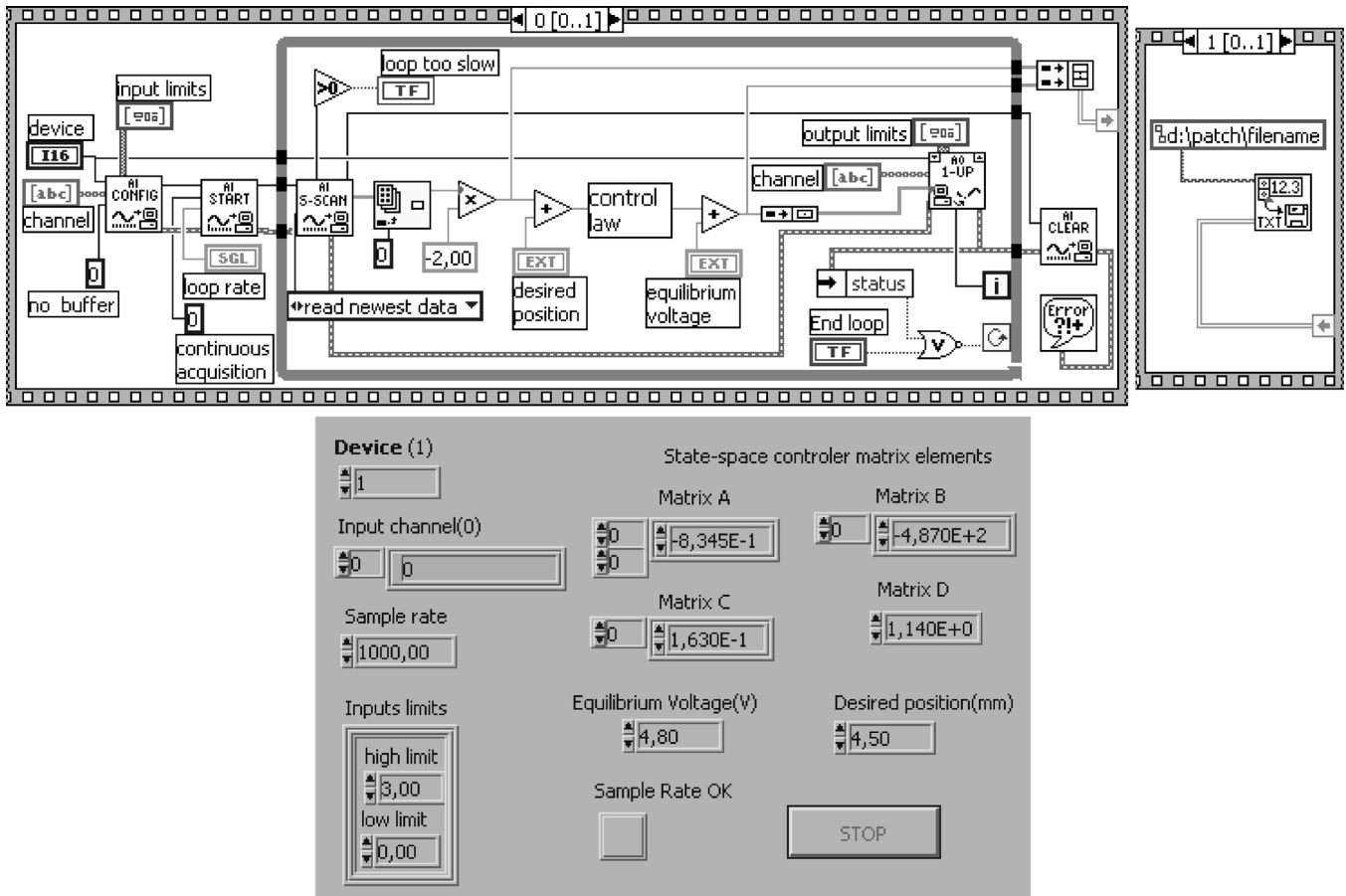
Fig. 11. LabVIEW sequence subdiagrams (upper) and front panel (bottom).

is used. The LabVIEW presents great flexibility but executes more slowly than the assembly or C language routines. The maglev control routine implemented as a sequence of two subdiagrams achieved the real time processing with conventional data acquisition hardware in a Pentium III PC. This procedure was possible provided the control process is the only task being performed. Fig. 11 shows the block diagrams and panel used in the experiment. In the former, the controller enters in the block-named control law. These block diagrams and the controller matrices used are available at the Web address http://www.sel.eesc.usp.br/rtsel [16]. There are several textbooks in digital control theory. (For a comprehensive account on the subject, see [17] and [18]. In the latter, the fundamentals of LabVIEW programming to implement digital control are also given.)

B. Experimental Setup

The basic configuration of the system hardware for digital control is composed of an acquisition board of the family 6020E with a 12-bit 12-kHz A/D converter and a 12-bit digital–analog (D/A) converter from National Instruments installed in an ISA-Bus of a standard Pentium III-CPU-based 800-MHz microcomputer. The position sensor output is connected to a 5B series conditioner board in a 5B41 voltage input module which accepts ± 10 V and provides ± 5 V. The analog output from a D/A converter is connected to the power amplifier module

described before. The input and output signals are connected via a 50-pin cable and a SC20-50 board. The complete control system diagram is shown in Fig. 12.

C. Experimental Results

Taking into account the maglev system fast time constant, which is about 20 ms, the sampling time, denoted T, is selected as 1 ms. Following are the functions used to generate the discrete controller K found in Sections V-C and V-D.

$$[\texttt{syscd}] = \texttt{bilin}(\texttt{K}, 1, \text{`tustin'}, \texttt{T});$$
$$/*\texttt{converts to discrete form}*/$$
$$[\texttt{Ac}, \texttt{Bc}, \texttt{Cc}, \texttt{Dc}, \texttt{T}] = \texttt{ssdata}(\texttt{syscd});$$
$$/*\texttt{generates the system matrices}*/$$

To illustrate the results, step disturbances are applied after positioning the steel ball about the adopted equilibrium (h_0, i_0). The step disturbance is set in the LabVIEW panel by altering the voltage v sent to the coil. The experiment is thus repeated with mass variations about 7% and 25% of its nominal value to investigate the robustness of the system with respect to variations in the mass of the steel ball. Different step disturbances are also considered.

D. Experimental Evaluation

The experimental results obtained are shown in Figs. 13–15, which are in good agreement with the corresponding simulation
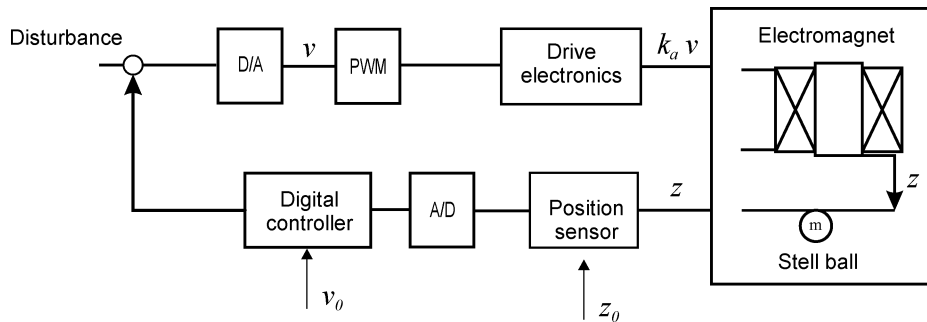
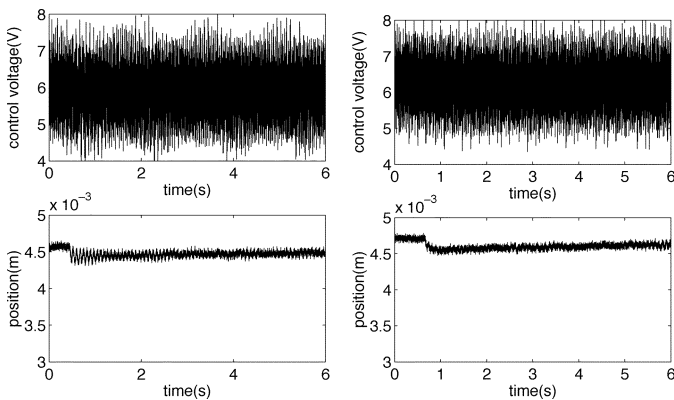Fig. 12.   Components of the maglev control system.

Fig. 13.   System responses for a 0.1 V disturbance step with a lead–lag controller without mass variation (left) and with 7% variation of the mass (right).
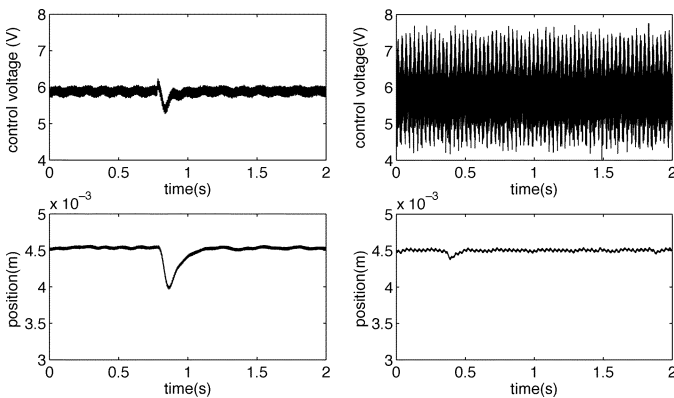

Fig. 15.   System responses for a 0.7-V disturbance step with the H_∞ controller (left) and μ controller (right).

Fig. 14.   System responses for a 0.5-V disturbance step with the H_∞ controller (left) and μ controller (right) for 25% variation of the mass.

results shown in Figs. 16–18. In Fig. 15 (left), the large effect of a high step disturbance on the equilibrium position exceeds the linear range of the sensor, deteriorating the system performance. However, this effect does not occur with the μ controller, as illustrated in Fig. 15 (right), which indicates that this controller produced an appropriate action fast enough to avoid large deviations on the steel ball position. The lead–lag controller could not stabilize the plant for large variations on the mass and disturbance. The plots shown were obtained from the experiment data written in a file.

From Figs. 13–15, one sees that the robust controllers achieve better disturbance rejection than the lead-lag controller and that the robust controllers perform very well in bringing the ball back
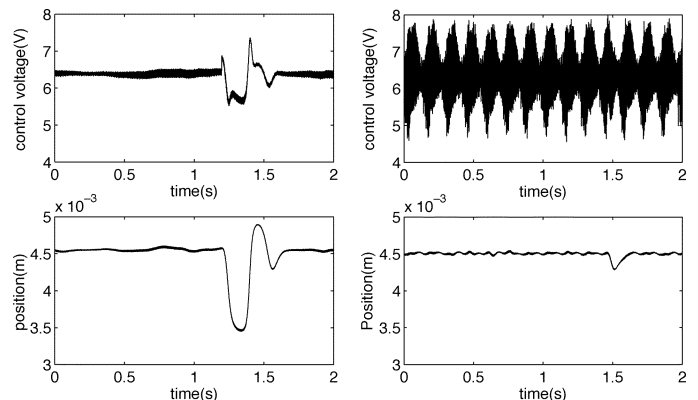
to the adopted operating position even when the system is subjected to changes in the mass m. With the robust controllers, in accordance with the robustness tests carried out using μ analysis, the design specifications are met for other steel balls of different sizes and mass. Moreover, the μ controller showed better disturbance attenuation responses when compared with the standard H_∞ controller responses. However, the μ controller is not as efficient as the standard H_∞ controller in suppressing the control signal noise, for it presents a higher gain. The conclusion is that the μ controller design is more conservative with respect to disturbances.
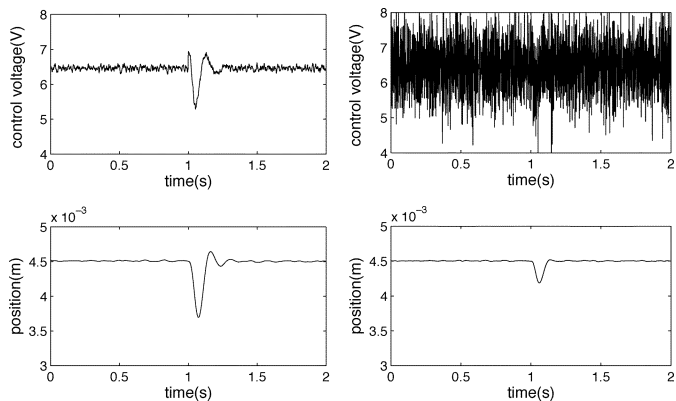
One should note here that simpler controllers obtained by following a tuning procedure perform well in many industry applications. This fact explains the popularity of the well-known tree term proportional plus integral plus derivative (PID) controller. However, in some applications the best performance attainable by a simpler controller is inadequate. More complex controllers, such as the ones addressed in this paper, should overcome this limitation but at a higher cost in terms of both implementation and designer's time.

VIII. STUDENT FEEDBACK

In general, the responses of students to the proposed interactive class activities were quite positive. The course is developed in 25 hours, and the classroom seats up to 25 students. Student comments indicate that the introduction of robust techniques with focus on applications relating control theory, simulation, and laboratory work along with the use of nonlinear
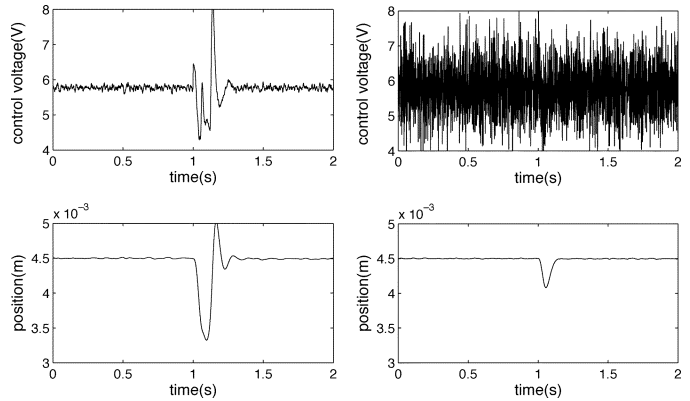
TABLE I
STUDENT FEEDBACK

Ratings: 5 = excellent, 1 =poor	5	4	3	2	1
Relevance of the course in the curriculum	25%	50%	8%	17%	0%
Benefit from supervised extra class work in learning control concepts	83%	17%	0%	0%	0%
Experience gained with MATLAB/Simulink in class work	42%	50%	8%	0%	0%
Global evaluation	75%	17%	8%	0%	0%
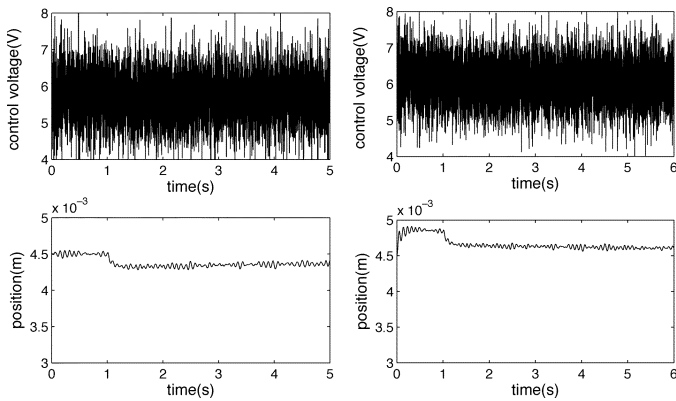
Fig. 16. Simulated responses for a 0.1-V disturbance step and white noise variance of 1e-6 with a lead–lag controller without mass variation (left) and with 7% variation of the mass (right).

Fig. 18. Simulated responses for a 0.7-V disturbance step and white noise variance of 0.1e-6 with the H_∞ controller (left) and μ controller (right).

Fig. 17. Simulated responses for a 0.5-V disturbance step and white noise variance of 0.1e-7 with the H_∞ controller (left) and μ controller (right) for 25% variation of the mass.

project reveals new control components and applications to the students. The use of frequency response techniques to describe the performance specifications and the use of Simulink to obtain the augmented plant were very well taken by the students. The LabVIEW VI in the configuration used is provided so that the students only need to replace the designed controller parameters in the control law block as shown in Fig. 11.

IX. CONCLUDING REMARKS

A simple laboratory experiment using MATLAB and LabVIEW has shown the applicability of recent robust control tools. The test for robustness using μ analysis provided insights into the limitations of controller designs. Design and implementation steps, including the modeling of the control problem with weighting functions and LabVIEW programming, are described in detail to facilitate the reproduction of the experiment. To achieve the objectives of the course three types of assessment are used: an individual presentation of homework solutions, a group presentation of a final course project, and a final individual test. To cope with large nonlinear regimes, the maglev device used needs some improvement. In this direction, the use of photodiode arrays in place of the single phototransistor employed for the position detection is at the present time being researched.

equations in the simulations was considered the strong points of the course. In addition, the majority of the students remarked that the intensive use of MATLAB and Simulink in class contributed to further develop their skills in computational tools. A summary of the latest postcourse student evaluations is provided in Table I. Only 12 surveys were used since this particular course is chosen mainly by the students enrolled for the Instrumentation and Control Certificate offered by the Universidade de São Paulo at São Carlos, Brazil.

As a consequence of the experience gained in class activities after some lectures, the participation of students in discussions improved. Moreover, as each group explores more strongly some aspects of the project according to their ability and involvement with other disciplines, the multidisciplinarity of the

REFERENCES

[1] J. Burl, *Linear Optimal Control: H_2 and H_∞ Methods.* Menlo Park, CA: Addison-Wesley, 1999.

[2] R. C. Dorf and R. H. Bishop, *Modern Control Systems.* New York: Prentice-Hall, 2000.

[3] P. N. Paraskevopoulos, *Modern Control Engineering.* New York: Marcel Dekker, 2002.

[4] D. P. P. S. Shiakolas, "Development of a real-time digital control system with a hardware-in-the-loop magnetic levitation device for reinforcement of controls education," *IEEE Trans. Educ.*, vol. 46, no. 1, pp. 79–87, Feb. 2003.

[5] W. G. Hurley and W. H. Wolfle, "PWM control of a magnetic suspension system," *IEEE Trans. Educ.*, vol. 47, no. 2, pp. 165–173, May 2004.

[6] P. S. Shiakolas, S. R. V. Schenck, D. Piyabongkam, and I. Frangeskou, "Magnetic levitation hardware-in-the-loop and MATLAB-based experiments for reinforcement of neural network control concepts," *IEEE Trans. Educ.*, vol. 47, no. 1, pp. 33–41, Feb. 2004.

[7] K. Zhou, *Essentials of Robust Control*. Upper Saddle River, NJ: Prentice-Hall, 1998.

[8] R. Y. Chiang and M. G. Safonov, *Robust Control Toolbox User Guide*. Natick, MA: The MathWorks, Inc., 1996.

[9] K. Zhou, J. C. Doyle, and K. Glover, *Robust and Optimal Control*. New York: Prentice-Hall, 1996.

[10] J. C. Doyle and K. Glover, *Robust and Optimal Control*. New York: Prentice-Hall, 1996.

[11] M. G. Safonov, "Stability margins of diagonally perturbed multivariable feedback systems," presented at the IEEE Conf. Decision Control, San Diego, CA, 1981.

[12] T. H. Wong, "Design of a magnetic levitation control system—An undergraduate project," *IEEE Trans. Educ.*, vol. 29, no. 4, pp. 196–200, Nov. 1986.

[13] V. A. Oliveira, E. F. Costa, and J. B. Vargas, "Digital implementation of a magnetic suspension control system for laboratory experiments," *IEEE Trans. Educ.*, vol. 42, no. 4, pp. 315–322, Nov. 1999.

[14] A. Bittar and R. Sales, " H_2 and H_∞ control for maglev vehicles," *IEEE Control Syst. Mag.*, vol. 18, no. 4, pp. 18–25, Aug. 1998.

[15] G. J. Balas, J. C. Doyle, K. Glover, A. Packard, and R. Smith, *μ Analysis and Synthesis Toolbox User Guide*. Natick, MA: The MathWorks, Inc., 1995.

[16] E. S. Tognetti, D. Siqueira, and V. A. Oliveira, Experimentos de controle avançado usando síntese μ Apr. 2004 [Online]. Available: htpp://www.sel.eesc.sc.usp.br/rtsel/, Tech. Rep.

[17] K. Ogata, *Discrete Time Control Systems*. Upper Saddle River, NJ: Prentice-Hall, 1995.

[18] C. L. Phillips and H. T. Nagle, *Digital Control System Analysis and Design*. Upper Saddle River, NJ: Prentice-Hall, 1995.

Vilma A. Oliveira (M'94) received the B.Eng. degree in electronics from the Universidade do Estado do Rio de Janeiro, Brazil, in 1976, the M.Sc. degree in electrical engineering from the Universidade Federal do Rio de Janeiro, Brazil, in 1980, and the Ph.D. degree in electrical engineering from the University of Southampton, U.K., in 1989.

She joined the Departamento de Engenharia Elétrica, Universidade de São Paulo, Brazil, in 1990, where she is currently a Full Professor. Her research interests include control design and applications.

Eduardo S. Tognetti received the B.S. and M.S. degrees in electrical engineering from the Escola de Engenharia de São Carlos, Universidade de São Paulo, São Carlos, Brazil, in 2002 and 2006, respectively.

He is currently a Control System Engineer at Votorantim Celulose e Papel, Piracicaba, São Paulo, Brazil, working on plant information management systems (PIMS) and control loop optimization. His research interests include control theory, robust control and uncertain systems, linear matrix inequalities, control loop optimization, and plant information management systems.

Daniel Siqueira received the B.S. degree in electrical engineering from the Escola de Engenharia de São Carlos, Universidade de São Paulo, São Carlos, Brazil, in 2003. He is currently working towards the M.S. degree at the Instituto de Tecnologia de Aeronáutica, São José dos Campos, Brazil.

His research interests include flight dynamics, robust control, and uncertain systems.